



THE UNIVERSITY *of* EDINBURGH

Edinburgh Research Explorer

## Numerical and Experimental Investigation of Joule Heating in a Carbon Fibre Powder Epoxy Towpregging Line

### Citation for published version:

Celik, M, Maguire, J, Noble, T, Robert, C & Ó Brádaigh, CM 2022, 'Numerical and Experimental Investigation of Joule Heating in a Carbon Fibre Powder Epoxy Towpregging Line', *Composites Part A: Applied Science and Manufacturing*, vol. 164, 107285. <https://doi.org/10.1016/j.compositesa.2022.107285>

### Digital Object Identifier (DOI):

[10.1016/j.compositesa.2022.107285](https://doi.org/10.1016/j.compositesa.2022.107285)

### Link:

[Link to publication record in Edinburgh Research Explorer](#)

### Document Version:

Peer reviewed version

### Published In:

Composites Part A: Applied Science and Manufacturing

### General rights

Copyright for the publications made accessible via the Edinburgh Research Explorer is retained by the author(s) and / or other copyright owners and it is a condition of accessing these publications that users recognise and abide by the legal requirements associated with these rights.

### Take down policy

The University of Edinburgh has made every reasonable effort to ensure that Edinburgh Research Explorer content complies with UK legislation. If you believe that the public display of this file breaches copyright please contact [openaccess@ed.ac.uk](mailto:openaccess@ed.ac.uk) providing details, and we will remove access to the work immediately and investigate your claim.



# Numerical and Experimental Investigation of Joule Heating in a Carbon Fibre Powder Epoxy Towpregging Line

Murat Çelik\*, James Maguire, Thomas Noble, Colin Robert, Conchúr M. Ó Brádaigh

School of Engineering, Institute for Materials and Processes, The University of Edinburgh, Sanderson Building, King's Buildings, Edinburgh, EH9 3FB, UK

*\*corresponding author, e-mail address: m.celik@ed.ac.uk*

## Abstract

Powder epoxy based towpregs offer favourable processing and storage properties, thanks to the low viscosity and thermal stability of the powder epoxy. Low-cost, high-quality towpregs, which are suitable for automated fibre placement or filament winding applications, can be produced at a high production rate with an automated towpregging line. This study focuses on improving the towpregging process by analysing the heating characteristics of a towpregging line that employs Joule heating to impregnate carbon fibre tows with powder epoxy. A finite element analysis heat transfer model was developed to identify the relationship between processing parameters and heating of the carbon fibre tows. Model predictions matched well with experimental results. Using the temperature distribution predicted by the model, powder epoxy melting and sintering behaviour was investigated using semi-empirical equations. Results revealed that Joule heating provides efficient heating with very low power consumption. It was found that while it is possible to produce towpregs at high production speeds (15 m/min), slower speeds might yield more consistent quality. Using parametric studies in the model, it was shown that it is possible to increase towpregging line production rate without compromising the towpreg quality, by altering some of the key process parameters (supplied current, electrode distance etc.).

## 1. Introduction

The composites industry has benefited immensely from automated manufacturing methods in recent years, for instance, up to 85% reduction in labour hours was reported by companies [1]. Methods such as automated fibre placement (AFP), which is an additive manufacturing process in essence, can produce composite parts at high rates with minimal material waste and error. Repeatability and accuracy of such systems are appealing to many industries [2].

In the AFP process, narrow-width prepreg tapes (towpreg) are laid on a mould layer by layer, and are consolidated with heat and pressure application by the AFP head. AFP applications are expected to play a major role in the future, especially if the current technology keeps up with the recent advances in Industry 4.0 [3]. In line with the progress in the AFP process, there is a growing interest in the materials that are used in AFP: towpregs (or prepreg tape) are one of the fastest-growing type of prepreg materials in the composite market [4]. Typically, towpreg manufacture is carried out using production lines, which can adopt melt-

36 impregnation [5]–[9], powder slurry [10]–[12] or powder coating [13]–[20] techniques in order to impregnate  
37 the powder with the thermoplastic or thermoset matrix. Although AFP is a cost-effective process, conventional  
38 towpreg can be expensive. In order to reduce material costs while maintaining the quality, powder epoxy-based  
39 towpregs have been developed [21], [22]. The towpregging line, or tapeline, developed by Robert et al. [21]  
40 impregnates carbon fibre tows with a novel powder epoxy. Powder epoxy composites do not require  
41 refrigerated storage conditions and have a long shelf life at room temperature, thanks to their chemical stability  
42 at room temperature [23]. From a processing perspective, the low viscosity of the molten powder epoxy results  
43 in good consolidation of the final part and relatively little heat generation when curing, minimising the risk of  
44 thermal runaway. Furthermore, little or no volatile organic compounds (VOCs) are released, and the excess  
45 powder can be recycled.

46 In the tapeline system [21], powder epoxy is deposited on the carbon fibre tow and melted by heating the  
47 tow through Joule (resistive) heating. Conductive carbon fibres heat up and act as individual heating elements  
48 when a current passes through, thus uniform and rapid heating can be achieved via Joule heating. It can be  
49 used in composite applications, particularly in the curing of composites, due to its simplicity, effectiveness,  
50 and efficiency. The power consumption of Joule heating is extremely low when compared to conventional  
51 heating systems, up to 80% lower power consumption than oven heating was reported [24], while comparable  
52 mechanical performance was obtained. It was shown that even some mechanical properties can be improved  
53 by Joule heating; Sierakowski et al. [25] demonstrated that it is possible to enhance the impact resistance of  
54 the composites by applying DC for short periods. One of the most advantageous features of this technique is  
55 uniformity in the temperature, which results in a consistent degree of curing along the part. Although local  
56 thermal gradients might be observed in electrode-composite interfaces [26], a uniform temperature profile over  
57 the sample can be attained in Joule heating systems [27]. Furthermore, overall curing time is much shorter [28]  
58 since heat is generated directly in the carbon fibres. This contrasts with oven heating, where the air inside must  
59 be heated first before heat transfers to the composite part. Degrees of curing of parts heated with Joule heating  
60 can exceed oven-cured composite parts [29]. Other than curing, some practical applications are compatible  
61 with Joule heating, including self-healing [30]–[33] and de-icing [28], [34]. Contact resistances occurring at  
62 the electrode-composite interfaces, however, create thermal gradients and therefore must be taken into account  
63 when designing heating systems.

64 Modelling methods are extensively used for calculating the heat generated by the Joule effect [25], [33],  
65 [35]–[38]. Calculating the temperature field through numerical models can improve mould design by  
66 visualising the thermal gradients. Furthermore, by coupling other process models, one can gain insight into  
67 different physics during the manufacturing, such as the curing or crystallisation behaviour of the material. With  
68 appropriate boundary conditions, temperature distribution during the Joule heating of composites can be  
69 calculated accurately [36]. As mentioned before, however, contact resistances must be defined carefully as  
70 they can be responsible for significant non-uniformities near electrode-composite interfaces [26]. It is possible  
71 to account for this additional heating by characterising the contact resistances. Sierakowski et al. [25]  
72 demonstrated that the heating caused by contact resistances can be more significant than Joule heating for  
73 longer heating durations. Kwok and Hahn [33] accounted for the contact resistance heating in their model by

74 introducing a thin, high resistance layer at the electrode/composite interface. Although their model overpredicts  
75 the temperature of the specimen greatly, it performed well in estimating the local hot spots. The authors  
76 claimed that the deviation is due to the actual resistivity of the material being different from the one used in  
77 the model. Similar deviations are common in Joule heating models [37], [38], mainly caused by ill-defined  
78 material properties. Lu et al. [39] used a heat transfer model to analyse the heat losses occurring in a continuous  
79 polyacrylonitrile-carbon nanotube stabilisation system. They found out that, by utilising Joule heating, the  
80 stabilisation duration can be reduced from 2.5 hours to under 1 hour, with only 1% of the power requirement  
81 of convective heating.

82 While the tapeline system can benefit from a heat transfer model, understanding the melting behaviour of  
83 the powder epoxy is equally important and can improve production. Melting and sintering of polymer powders  
84 have been explored both experimentally and numerically [40]–[44]. With an increase in temperature, powder  
85 polymer melting is followed by sintering, which is a double-stage mechanism including powder coalescence  
86 and bubble removal [43]. It is a widely discussed topic for rotational moulding and laser sintering applications  
87 [40], [42], however, Maguire et al. [23] described the sintering of the powder epoxy for thick-section composite  
88 manufacturing, using a semi-empirical equation. From the towpreg manufacturing standpoint, it is vital to  
89 ensure that the state of the powder epoxy during the heating is optimal to provide a good degree of  
90 impregnation. By coupling heat transfer models to appropriate melting and sintering models, the ideal  
91 processing window for the manufacturing of towpregs can be determined.

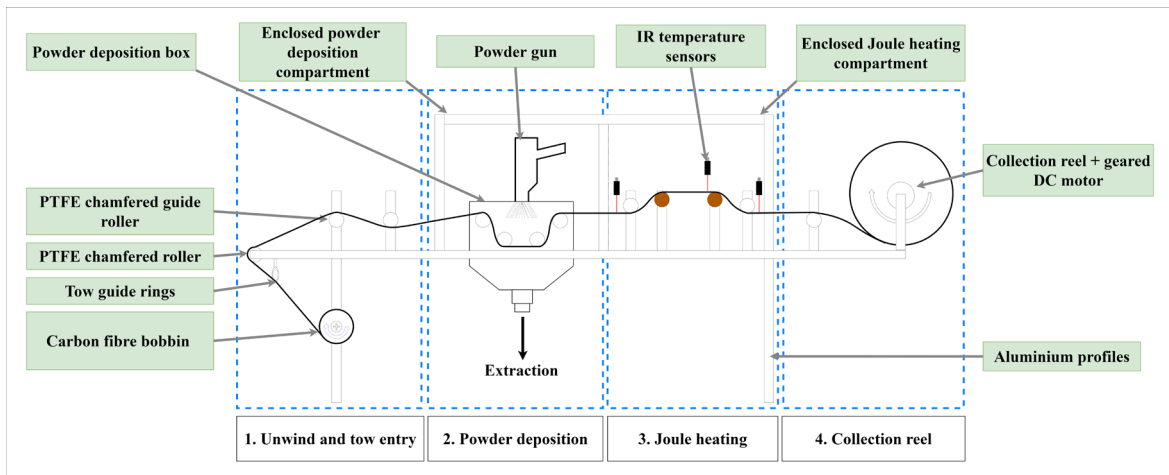
92 Most of the towpregging systems include a crucial heating step in the production line, either to preheat  
93 fibres before the impregnation step or to melt the deposited matrix or removal of the solvent after the  
94 impregnation step [5]–[20]. Thermal models of such systems provide a better understanding of the overall  
95 process and the possibility to analyse the system in detail. [10]. Most of the aforementioned studies, however,  
96 sought to investigate the towpregging processes from an experimental point of view, and the developed thermal  
97 models are limited in capacity [10]. The authors previously identified the contact resistances in the Joule  
98 heating system of the tapeline in an experimental campaign, and through a simplified finite element analysis  
99 (FEA) model, they demonstrated that the accuracy of thermal models can be improved by accounting for  
100 contact resistances [45]. This paper aims to characterise the Joule heating process through a parametric thermal  
101 model supported by experimental data. Not only is the manufacturing process analysed by modelling beyond  
102 experimental limitations (power input, electrode distance etc.), but also the on-line melting and sintering  
103 behaviour of the powder epoxy is predicted, which is quite difficult to accomplish using experimental  
104 techniques. Thus, our study can be of interest to a broader community, in terms of experimental and modelling  
105 perspectives, considering the recent interest in towpreg/prepreg tape manufacturing processes [5]–[20].  
106 Furthermore, similar modelling approaches can be used in different applications, such as well-known  
107 pultrusion [46]–[48], or niche applications such as double belt press lamination [49], localised in-plane thermal  
108 assist (LITA) technique [50], [51] and radio-frequency (RF) heating [52].

## 109 **2. Experimental**

### 110 *2.1. Tapeline system*

111 A tapeline system has been developed [21] to produce low-cost, high-quality and fully consolidated (but  
 112 not cured) powder epoxy-based towpregs that are compatible with AFP applications. In this system, carbon  
 113 fibre tows are pulled through a series of rollers, powder epoxy is electrostatically deposited on the carbon fibre  
 114 tow using a charged epoxy powder particle cloud in a semi-confined box under constant extraction. Joule  
 115 heating is used to heat the carbon fibre tow and to melt the powder epoxy, and finally the produced towpreg is  
 116 collected (Figure 1). A detailed description of the system is provided in [21], [22]. The main advantage of the  
 117 tapeline system is that the towpreg production is automated and is monitored by various sensors (tow tension,  
 118 temperature, speed etc.), allowing for high-volume production of high-quality towpregs. The towpregging line  
 119 includes an active tension control system, which uses tension sensors to monitor the tension of the tow at all  
 120 times and a PID-controlled magnetic brake to maintain a set tension on the tow, based on the data read from  
 121 the tension sensor. Therefore, the tension of the tow remains constant throughout a production run. The  
 122 advantageous processing properties of the powder epoxy include low viscosity, no VOCs, easy deposition and  
 123 long storage life. By altering the operating parameters of the tapeline, different fibre volume fractions (and  
 124 consequently different mechanical properties) can be achieved. Furthermore, another key advantage of the  
 125 towpregging line is its versatility. With some alterations in the system, thermoplastics powders could be used  
 126 for towpreg production, which would attract great interest due to their recyclability. Although for some  
 127 thermoplastics, such as PEEK, the processing window between melt and degradation is very narrow, as the  
 128 heating time is very short in the line, working with such materials could be achievable.

129



130

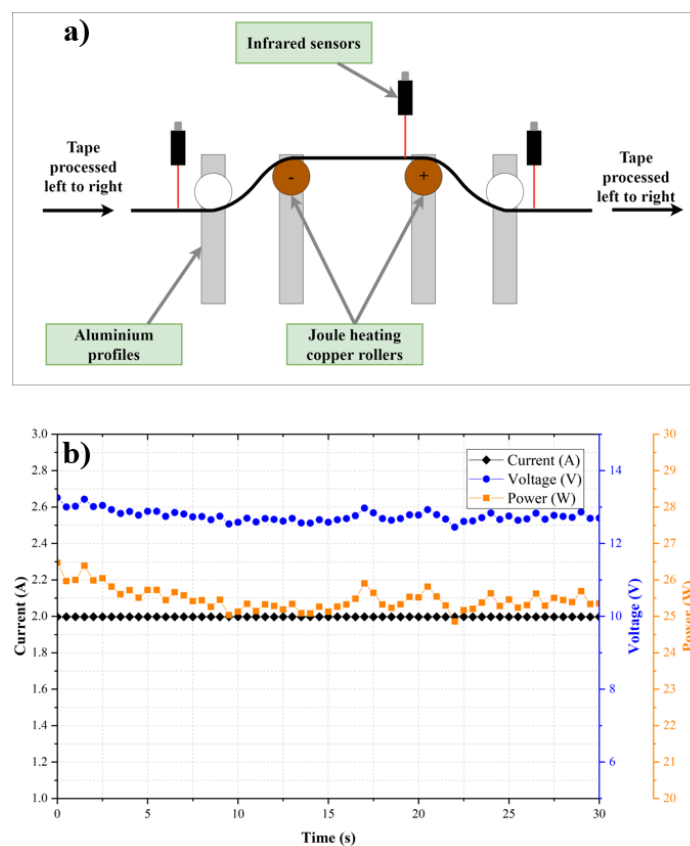
131 **Figure 1.** Schematic of the tapeline.

132

133 *2.2. Joule heating*

134 Joule heating is the preferred option in the tapeline system for heating the carbon fibre tows and is carried  
 135 out after powder deposition, in order to melt the powder epoxy deposited on the tows. Two conductive copper  
 136 roller electrodes are used to provide the electrical current, while infrared (IR) temperature sensors (OS-PC30-

137 2M-1V, OMEGA Engineering) measure the temperature of the tows constantly (Figure 2a). Based on the IR  
 138 temperature sensor data, a PID controller adjusts the current passing through the carbon fibre to reach the set  
 139 temperature. Joule heating provides rapid heating of the carbon fibre tows (e.g. 4 seconds to reach 120°C) and  
 140 the power requirement is also very small, as shown in Figure 2b (around 25 W), whereas a small curing oven  
 141 typically operates at 500 W [24]. There is no further equipment required apart from the conductive rollers and  
 142 PID control system, and instantaneous automated temperature control is possible with the Joule heating system.  
 143 Powder epoxy and loose carbon fibre filaments can, however, build up around the conductive rollers during  
 144 prolonged production runs, which can prevent the current from flowing through the fibres, resulting in  
 145 disruptions in the production. To avoid powder epoxy and loose carbon fibre build up around the rollers, metal  
 146 scrapers were placed underneath the copper rollers.



147

148 **Figure 2. a)** The heating section of the tapeline **b)** typical current, voltage and  
 149 power characteristics during heating

150

151 *2.3. Materials*

152 Toray T700S-24K-50C (1% sizing) carbon fibre tow and powder epoxy (PE6405, 1220 kg/m<sup>3</sup>, supplied  
 153 by FreiLacke and designed by Swiss CMT AG) were used for the towpreg production. The conductive Joule  
 154 heating electrodes were made of copper. Slip-rings were fitted inside the copper electrodes to provide electric

155 current. An infrared thermal camera (FLIR A655SC) was used to measure the temperature distribution in the  
 156 carbon fibre tow.

### 157 3. Numerical Modelling

#### 158 3.1. Heat transfer model

159 Carbon fibre filaments in the tow act as heating elements when an electric current passes through, due to  
 160 the Joule effect. The additional heat due to the Joule heating term can be expressed as [25]:

$$161 \quad Q_{JH} = \frac{I^2}{\sigma V} \quad (1)$$

162 where  $Q_{JH}$  is the heat generated by the Joule heating ( $\text{W}/\text{m}^3$ ),  $I$  is the current provided (A),  $\sigma$  is the  
 163 electrical conductivity ( $\Omega$ ) and  $V$  is the volume of the medium ( $\text{m}^3$ ). The heat equation then becomes:

$$164 \quad c\rho \frac{\partial T}{\partial t} = \nabla(\mathbf{k}\nabla T) + Q_{JH} \quad (2)$$

165 where  $c$  is the specific heat capacity ( $\text{J}/\text{kg}\cdot\text{K}$ ),  $\rho$  is the density ( $\text{kg}/\text{m}^3$ ),  $T$  is the temperature (K),  $t$  is the  
 166 time (s) and  $\mathbf{k}$  is the thermal conductivity tensor of the carbon fibre tow ( $\text{W}/\text{m}\cdot\text{K}$ ).

167 At the interfaces between the carbon fibre tow and the electrodes, electrical contact resistances occur due  
 168 to the imperfect contact. A contact resistance heating term is used to describe this additional heating caused  
 169 by the electrical contact resistances, and can be expressed as [25]:

$$171 \quad Q_{CR} = \frac{I^2 R_{CR}}{A} \quad (3)$$

172 where  $Q_{CR}$  is the heat generated by the electrical contact resistances ( $\text{W}/\text{m}^2$ ),  $I$  is the current (A),  $R_{CR}$  is  
 173 the contact resistance ( $\Omega$ ) and  $A$  is the contact area of the interface ( $\text{m}^2$ ).

174

175

176

177

178 **Table 1:** Model parameters

Carbon fibre tow		Copper electrodes		Electrical properties	
Density [ $\text{kg}/\text{m}^3$ ] [53]	1800	Density [ $\text{kg}/\text{m}^3$ ] [54]	8960	Maximum applied current [A]	2

Specific heat [J/kg.K] [53]	752	Specific heat [J/kg.K] [54]	385	Electrical contact resistance layer thickness [mm]	0.1
Thermal conductivity in the axial direction [W/m.K] [53]	9.6	Thermal conductivity [W/m.K] [54]	400	Electrical conductivity in contact resistance layer [S/m]	2.3 - 10
Electrical conductivity in the axial direction [S/m]	42677	Electrical conductivity [S/m] [54]	5.99e7		
Linear velocity [m/s]	0.1083	Angular velocity [1/s]	10.83		
Width [mm]	6.35	Minimum wrap angle [°]	20		
Heated length [mm]	190	Width [mm]	98.5		
Thickness [mm]	0.2	Outer radius of the groove [mm]	10		
		Outer radius [mm]	16		
		Inner radius [mm]	4		

179

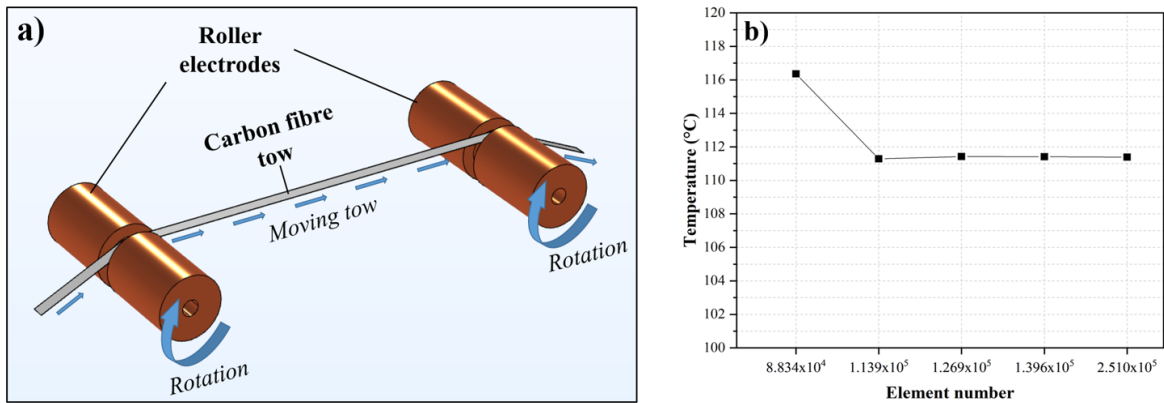
180

181 In order to solve the heat equation, a 3D time-dependent finite element model was developed using COMSOL  
 182 Multiphysics 5.6 software. Powder epoxy on the carbon fibre might lead to fluctuations in the temperature  
 183 during the production, hence dry carbon fibre (i.e. without the powder epoxy) was considered for heat transfer  
 184 modelling. The 3D domain created for the model is depicted in Figure 3a. The model uses an Eulerian domain  
 185 that accounts for the movement of the carbon fibre tow with a given production speed. Electrical contact  
 186 resistances occurring at the interfaces between the metal roller electrodes and the carbon fibre tows were  
 187 determined experimentally as explained in Ref [45]. The resistance of the entire system was measured for  
 188 different electrode distances, and resistance values were plotted against electrode distance. Assuming the linear



189 material resistivity, the y-intercept of the plots (zero electrode distance) were accepted as contact resistances  
 190 and cable resistance of the system. Similar approaches can be found in [30], [33], [55]. Electrical contact  
 191 resistance values obtained were applied to the contact areas at the interfaces by assigning an equivalent thin  
 192 layer in the contact patches. Model parameters were given in Table 1. A mesh convergence study was carried  
 193 out by increasing the element number in the domain as shown in Figure 3b.

194



195

196 **Figure 3. a)** Computational domain and **b)** mesh convergence plot for the model.

197

198 Due to the complex nature of the towpregging process, the following assumptions were made in the model:

- 199
- Thermal contact resistances were neglected.
  - 200 • For the heat transfer model, dry carbon fibre only (i.e. no powder epoxy on the surface) was modelled,  
 201 assuming powder-epoxy has no effect on the heating of the tow.
  - 202 • The speed, tension and power applied were constant, while some small fluctuations of such  
 203 parameters are observed during the production run.
  - 204 • Material properties (heat capacity, density, thermal conductivity etc.) are constant and not a function  
 205 of temperature.
  - 206 • A thin resistive layer was used at the contact patches to account for electrical contact resistances.
  - 207 • The carbon fibre tow is perfectly homogenous and solid, whereas in actuality, the tow characteristics  
 208 change along the length due to the high number of carbon fibre filaments (24K).
  - 209 • For the melting and sintering model, the powder epoxy on the tow is perfectly distributed and it is  
 210 present on every temperature node of the tow.

211

### 212 3.2. Melting and sintering model

213 Powder epoxy on the carbon fibre tows starts to melt when the temperature of the carbon fibre  
 214 exceeds the melting temperature of the powder epoxy. Further temperature increments lower the viscosity,  
 215 surface tension forces become dominant over the viscous forces, and the molten powder epoxy particles

216 coalesce into a homogenous melt, a process which is defined as sintering [43]. Molten and sintered powder  
 217 epoxy flows into the carbon fibre tow and upon cooling, solidifies, creating the towpreg. The sintering process  
 218 creates a homogenous layer of molten powder epoxy, by merging the randomly distributed resin sites, hence  
 219 the impregnation and consolidation of the resin are affected by the sintering of the powder epoxy. While it can  
 220 be seen visually whether the powder epoxy melts during the production, it is important to investigate the  
 221 melting and sintering behaviour further to improve production by better understanding the overall process.  
 222 Through numerical modelling, process parameters can be optimised, such as the heating section length to  
 223 ensure the powder is fully sintered. Thus, the heat transfer model was one-way coupled to the melting and  
 224 sintering model to account for the melting behaviour of the powder epoxy.

225 Maguire [56] carried out thorough characterisation studies on the powder epoxy, including  
 226 differential scanning calorimetry (DSC) and parallel plate rheometry (PPR) tests. By fitting Eq. 4, which was  
 227 proposed by Greco and Maffezzoli [43], to the DSC data, they were able to model the melting behaviour of  
 228 the powder epoxy:

$$229 \quad \frac{d\theta}{dt} = k_m e^{(-k_m(T-T_m))} [1 + (d-1)e^{(-k_m(T-T_m))}]^{d/(1-d)} \quad (4)$$

230 where  $T$  is the temperature,  $k_m$  and  $d$  are fitting parameters,  $T_m$  is the melting point and  $\theta$  is the  
 231 degree of melt. The values for the fitting parameters are presented in Table 2. By coupling the heat transfer  
 232 data to Eq. 4, it is possible to determine the degree of melting of the powder epoxy during the production run.

233 Similar to the melting model, Maguire et al. [23] also used parallel plate rheometry (PPR) test data  
 234 to relate powder sintering with thickness change, and demonstrated that sintering of the powder epoxy can be  
 235 modelled with a Williams-Landel-Ferry (WLF) type of equation:

$$236 \quad \frac{d\chi}{dt} = -\chi_0 \exp\left(\frac{C_{\chi 1}[T - T_\theta]}{C_{\chi 2} + T - T_\theta}\right) (\chi - \chi_\infty)^B \quad (5)$$

237 where  $\chi$  is the degree of sintering,  $\chi_0$  is the rate constant,  $\chi_\infty$  is the degree of sintering at infinity,  
 238  $C_{\chi 1}$ ,  $C_{\chi 2}$  and  $B$  are fitting constants,  $T$  is the temperature and  $T_\theta$  is the melting temperature. The constants were  
 239 found by fitting PPR results to Eq. 5, which are given in Table 2.

240

241 **Table 2:** Fitting constants for melting and sintering model, taken from Maguire [56]

Model	Fitting constants	Value
<i>Melting model</i>	$k_m$	1.83
	$d$	4.65
	$T_m$	313.58 [K]
<i>Sintering model</i>	$\chi_0$	3e-5
	$C_{\chi 1}$	11.5
	$C_{\chi 2}$	24.5

	$B$	0.5
	$\chi_{\infty}$	0
	$T_{\theta}$	313.58 [K]

242

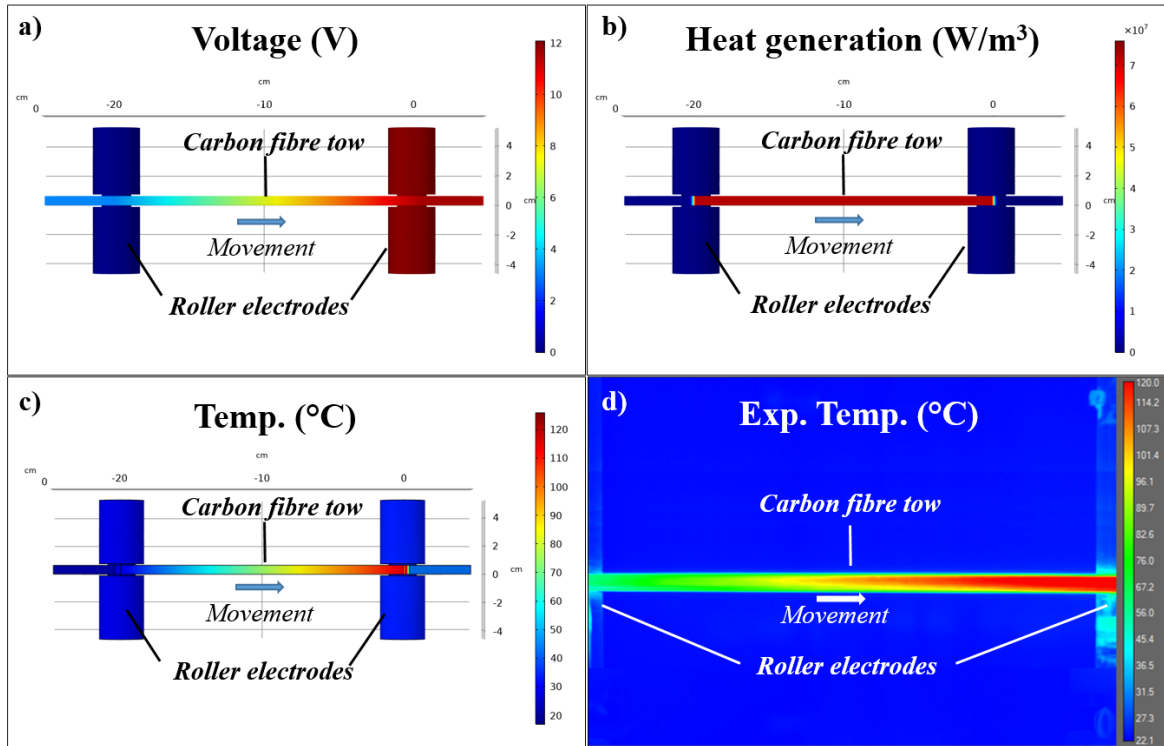
243

244 **4. Numerical Solution of Model, Validation and Discussion**

245 *4.1. Temperature distribution*

246 The temperature distribution of the tow was obtained from the heat transfer model that was solved using  
 247 COMSOL Multiphysics software. To check the validity of the model, thermal camera images of the Joule  
 248 heating system were used. The model findings were compared to the average temperature distribution of the  
 249 tow acquired experimentally by the thermal camera. Model predictions for voltage, heat generation and  
 250 temperature distribution for 2 A current, 20 N tension and 6.5 m/min production speed are presented in Figure  
 251 4, as well as the thermal camera image of the carbon fibre tow during the heating. Note that due to the reflective  
 252 surfaces of the roller electrodes, they are not visible in the thermal camera images. The agreement between the  
 253 model results and the experimental data is qualitatively good, however, a temperature gradient across the width  
 254 of the tow was observed from the thermal camera images. Furthermore, the model predicts a lower temperature  
 255 at the entry region to the heating section. These differences are most likely due to the higher temperatures  
 256 caused by the higher tension in the middle section of the tape. Higher tension in the centre of the tape improves  
 257 contact between fibres within the tow and also between the fibres and the copper rollers. Consequently, this  
 258 results in a local drop of electrical resistance and more current passes in the middle of the tow than the sides;  
 259 as the current prefers the least resistant path. Hence, temperature increases locally, and temperature gradients  
 260 are formed across the width.

261



262

263

264

265

266

267

268

269

270

271

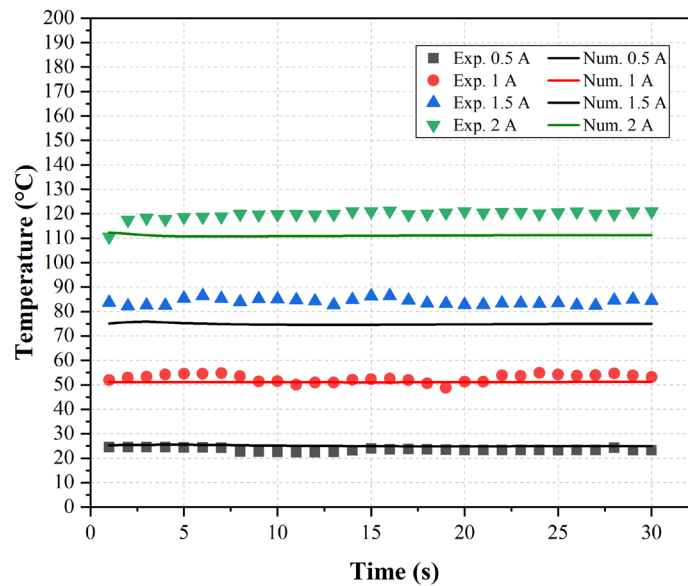
272

273

274

**Figure 4.** Model predictions for **a)** voltage **b)** heat generation and **c)** temperature distribution. **d)** thermal camera experimental image of the carbon fibre tow.

The current supplied to the heating system changes the maximum temperature reached in the carbon fibre tow. Figure 5 compares the average experimental and model prediction temperatures across the width of the tow, at the hottest region of the tow, for different supplied currents. A good agreement between the model and experimental values is observed at the 0.5 and 1 A currents. The model underpredicts the average temperature at higher current values, however, due to the aforementioned tension inconsistency across the width of the tow. The predicted average temperature by the model at 1.5 and 2 A is ~75°C and ~111°C, respectively, while the thermal camera measures the temperature at these currents as ~85°C and ~120°C. The difference between the actual average temperature and model prediction of maximum temperature region is under 8% in the processing window of towpreg, where the target temperature is around 120°C.



275

276

277

278

279

**Figure 5.** Comparison of experimental maximum temperatures with model predictions at different currents. Note that experimental temperatures are the average of the temperatures measured across the tow width at the point of maximum temperature

280

281

282

283

284

285

286

287

288

289

290

291

292

293

294

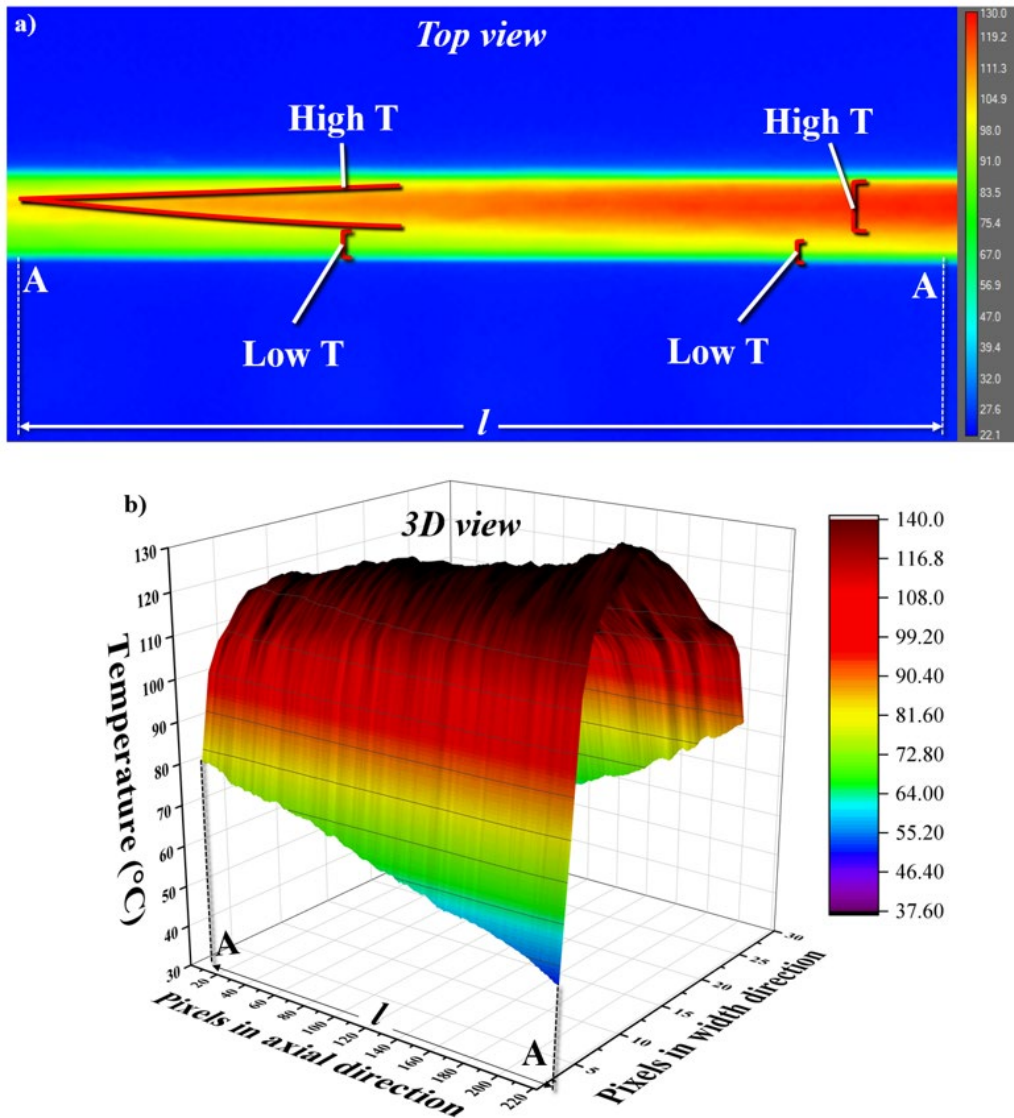
295

296

297

A typical thermal camera image is given in Figure 6, as well as surface plot of temperatures across the width at the hottest section of the tow. At a given time, tension can change momentarily across the width of the tow, due to a number of different factors, such as fibre packing, roller friction or a small lag during the unwinding from the spool. As explained earlier, the local variations of electrical resistance lead to high and low temperature regions as shown in Figure 6a. Generally, high temperature regions are near the centre of the tow, while the sides have a lower temperature (Figure 6b). Nevertheless, depending on the tension profile, high temperature regions can be observed at different places. The difference between the maximum and minimum temperature across the width can be significant, which is the reason why the model results were compared against the average temperatures in Figure 5. Localised high temperatures increase the average temperature, and as the model does not account for such tension difference across the width of the tow, the slight discrepancy between the model predictions and the experimental results was observed. Furthermore, the tow is inherently heterogeneous and the temperature profile might not be the same for all segments, along the length of the tow that is being heated. As a result of this, instantaneous random local temperature spikes were also observed in the tow (Figure 7) when a constant current is supplied. These variations are smaller when the average temperature across the tow width is considered, rather than a single point on the tow. In order to validate the numerical models, constant current was supplied in the heating zone, however, during the actual towpreg production, a PID controller is used to adjust the power input based on temperature readings. The PID

298 controller performs well in keeping the average temperature in a reasonable range for the towpreg production,  
299 by controlling the power input.

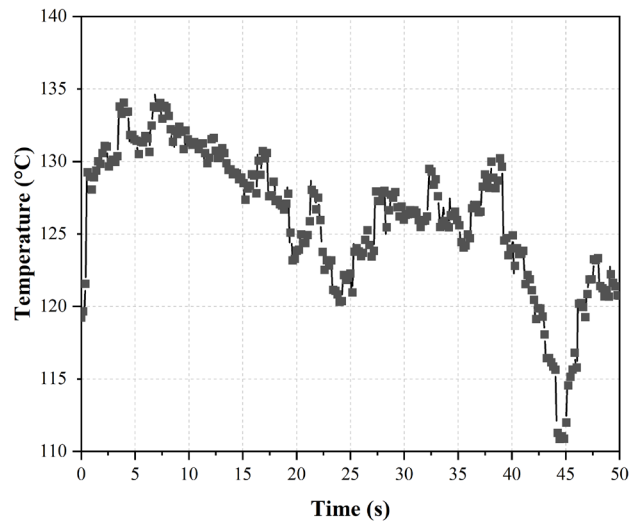


300

301 **Figure 6. a)** Experimental temperature variations across the width using an IR thermal camera  
302 (top view), a high temperature region near the top edge was formed. Note that rollers are out of  
303 field of view of the thermal camera. **b)** surface plot of the variations of temperature for the same  
304 area, captured by the IR thermal camera.

305

306



307

308

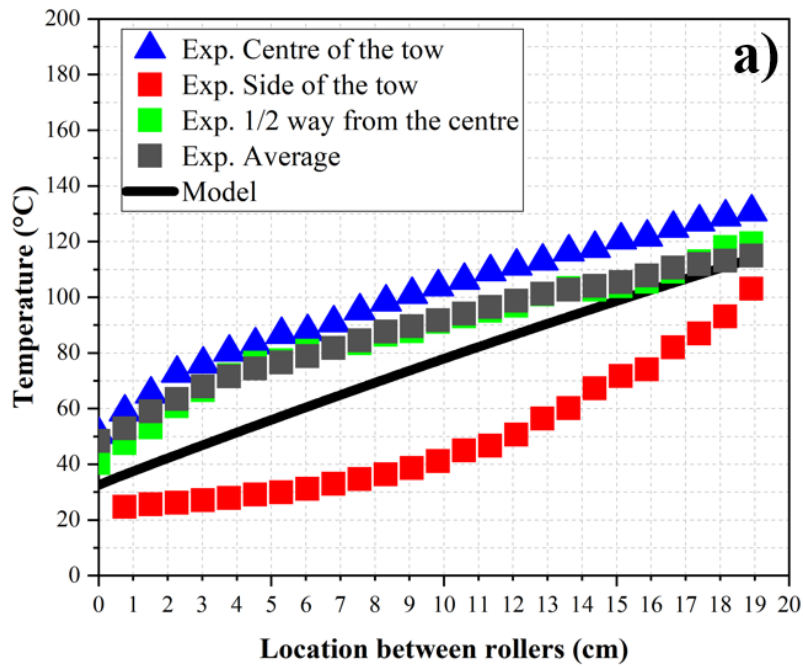
**Figure 7.** Local temperature fluctuations over time for a selected point on the tow

309

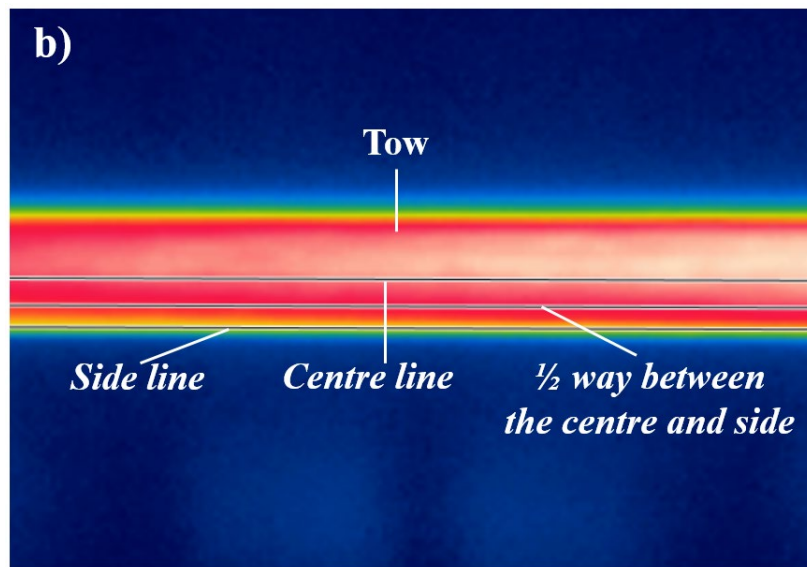
310 The model predictions of temperature along the tow in the heating zone and experimental measurements from  
 311 the centre and side of the tow are shown in Figure 8. A disparity was observed between the model and  
 312 experimental temperatures of the centre and side of the carbon fibre tow. This deviation was attributed to the  
 313 aforementioned uneven tension, and also to the fact that the model assumes a perfect thermal contact with the  
 314 rollers (i.e. no thermal contact resistances), which results in more heat transfer to the rollers than in the  
 315 experimental case. In terms of the towpregging production, the average temperature of the tow near the  
 316 maximum temperature region is the critical temperature for the complete melt of the powder epoxy, and the  
 317 model performs better for this temperature, as shown in Figure 5. Many Joule heating models have been  
 318 documented in the literature to have similar inaccuracies, especially at higher temperatures or currents [27],  
 319 [33], [37], [38]. Up to 40% higher predicted temperatures were presented by Chien et al. [37] for a Joule  
 320 heating model for polyacrylonitrile/carbon nanotube composite fibres, which they explained by referring to  
 321 inconsistency in fibre diameters, interfacial resistances between the nanotubes and polymer matrix, and altered  
 322 material properties at high temperatures. Kwok and Hahn [33] reported a major discrepancy between their  
 323 FEA model predictions and experimentally measured temperature values ( $>70^{\circ}\text{C}$ ) due to the difference in  
 324 actual and simulated resistivity values. Grohmann [38] presented a Joule heating model for a fibre placement  
 325 application, which overpredicted the temperatures 30% higher due to the actual material properties being  
 326 different from what was used in the model.

327

328



329  
330



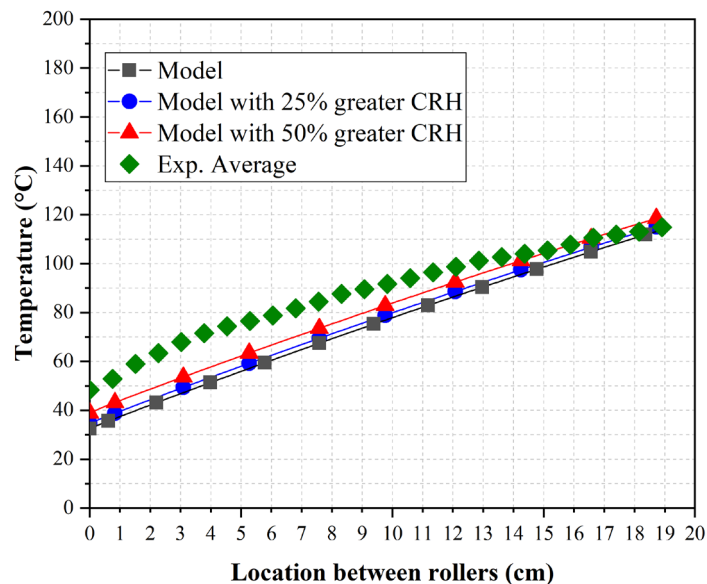
331  
332  
333  
334  
335

**Figure 8.** a) Comparison of model predictions of temperature along the tow with experimental temperatures from the centre and the side of the tow b) temperature measuring locations

336 One of the important phenomena observed in the Joule heating system of the tape is the effect of electrical  
337 contact resistances. Due to the imperfect contacts occurring between the carbon fibre tow and the copper  
338 rollers, electrical contact resistances occur and cause additional heating at the carbon fibre-roller surfaces. The  
339 influence of contact heating can be observed in the temperature distribution captured by the thermal camera.



340 Normally, in the heating section, one can expect a temperature gradient that begins from room temperature  
 341 near the beginning of the heated section (first roller electrode) and reaches the maximum temperature near the  
 342 second roller electrode. However, as shown in Figure 4d, the average temperature of the carbon fibre tow is  
 343 around 50°C when it enters the heating zone, indicating that the heating actually starts as soon as the carbon  
 344 fibre tow contacts the roller electrodes, due to the contact resistance heating (CRH) [45]. As previously  
 345 mentioned, electrical contact resistances were accounted for in the model by creating an equivalent resistant  
 346 thin film. Electrical contact resistance values for the corresponding operational conditions were determined  
 347 experimentally. By accounting for contact resistance heating, a similar trend was observed in the modelling  
 348 results, where the carbon fibre tow enters the heating zone already heated (Figure 4c and 4d). Likewise, the  
 349 temperature of the roller electrodes was also increased, as the heat generated by the contact resistance heating  
 350 diffuses through both the carbon fibre tow and the rollers. Interestingly, the presence of contact resistance  
 351 might be beneficial in terms of powder melt, due to the heating of the first roller electrode and a resulting  
 352 higher entrance region temperature of the tow. Figure 9 illustrates the influence of CRH on the temperature of  
 353 the tow, when plotted against the distance between the rollers. When the model calculates the temperature field  
 354 for 25% higher contact resistance heating, by defining a 25% more resistant thin film (1.77 S/m conductivity),  
 355 the agreement between the model and experimental results at the beginning of the heating zone improves. For  
 356 50% higher contact resistance heating (1.18 S/m conductivity), the agreement improves further, pointing out  
 357 the inaccuracy of neglecting thermal contact resistances in the model. It is highly likely that by assuming a  
 358 perfect thermal contact between the rollers and the carbon fibre tow in the model, heat transfer to the rollers is  
 359 overestimated, leading to a lower predicted temperature in the entry region.



360

361

362

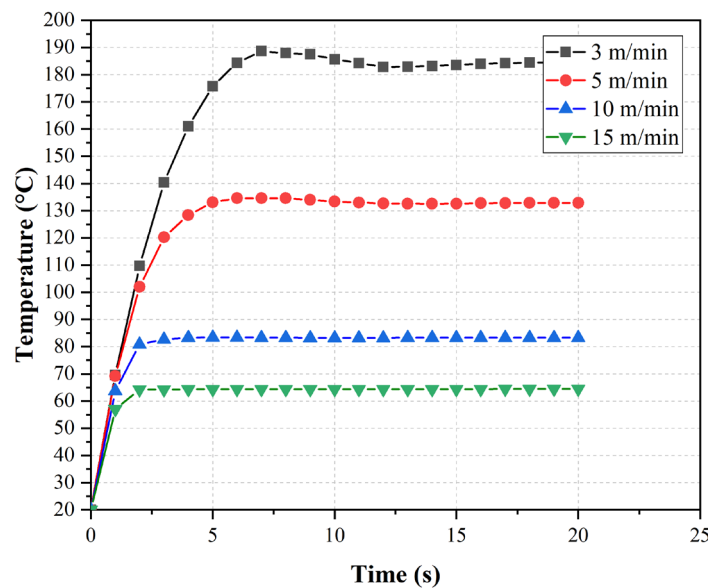
363

**Figure 9.** Comparison of the experimental average temperature of the tow in the heating zone against the model results with different contact resistance heating (CRH) values

364

365 *4.2. Parametric studies of the model on the effect of operating parameters on the temperature distribution*

366 While the aim of the presented towpreg production is to have a greater production rate with  
367 consistent quality, operating conditions have a substantial effect on the towpreg characteristics. For instance,  
368 higher production speeds mean that the carbon fibre tows spend less time in the powder deposition chamber,  
369 therefore, the amount of powder deposited changes with the production speed. Furthermore, the Joule heating  
370 time also reduces with high production speeds, consequently, for a given power input the maximum  
371 temperature reached is lower. Although powder epoxy has a relatively low melting temperature ( $\sim 40^{\circ}\text{C}$ ),  
372 higher operating temperatures are targeted in the heating section ( $\sim 100 - 120^{\circ}\text{C}$ ) to ensure the viscosity is  
373 minimal and good consolidation can be achieved without inducing significant cure. At high production speeds,  
374 these high temperatures may not be reached, so the power characteristics should be changed. The developed  
375 model was used to investigate the relationship between the production speed and the heating. Figure 10 shows  
376 the modelled temperature change with respect to the production speed for the same power characteristics (2 A,  
377 constant current). The maximum temperature changes from  $185^{\circ}\text{C}$  at 3 m/min to  $64^{\circ}\text{C}$  at 15 m/min for the  
378 same power input. In order to attain a low viscosity at higher production speeds, the current supplied should  
379 be increased correspondingly, and possibly the power source should be replaced with a higher capacity one.



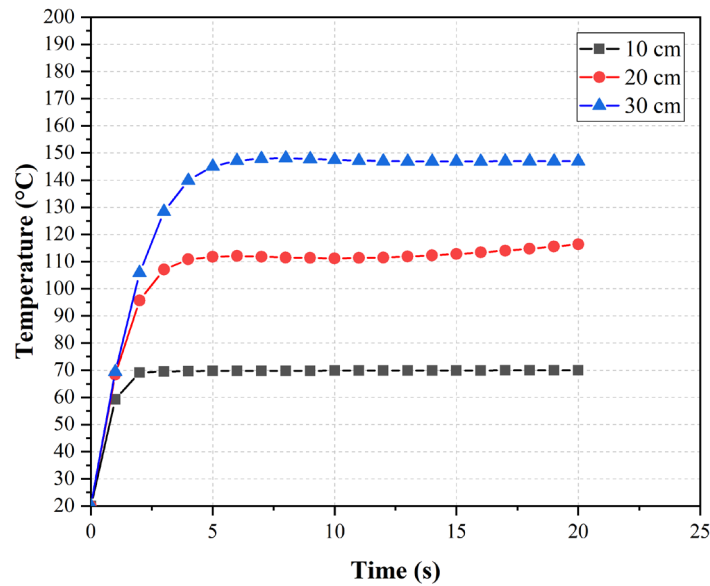
380

381 **Figure 10.** Modelled change of maximum tow temperature with respect to  
382 different production speeds at 2 A of constant current

383

384 Another alternative to reach targeted temperatures in the tapeline is to change the heating section length.  
385 This allows for a longer heating time for the tow, hence, the targeted temperature can be attained at lower

386 power input. If the heating section length is too small, the maximum temperature on the tape might not be  
 387 enough to fully melt the powder epoxy. It can be seen from model predictions in Figure 11 that at the same  
 388 current of 2 A, the maximum temperature of the tape changes remarkably with the electrode distance (i.e.  
 389 heating section length). Considering the dimensions of the heating section, an electrode distance of around 20  
 390 cm was deemed to be optimal in order to maintain the targeted temperature (120°C) for 2 A current.



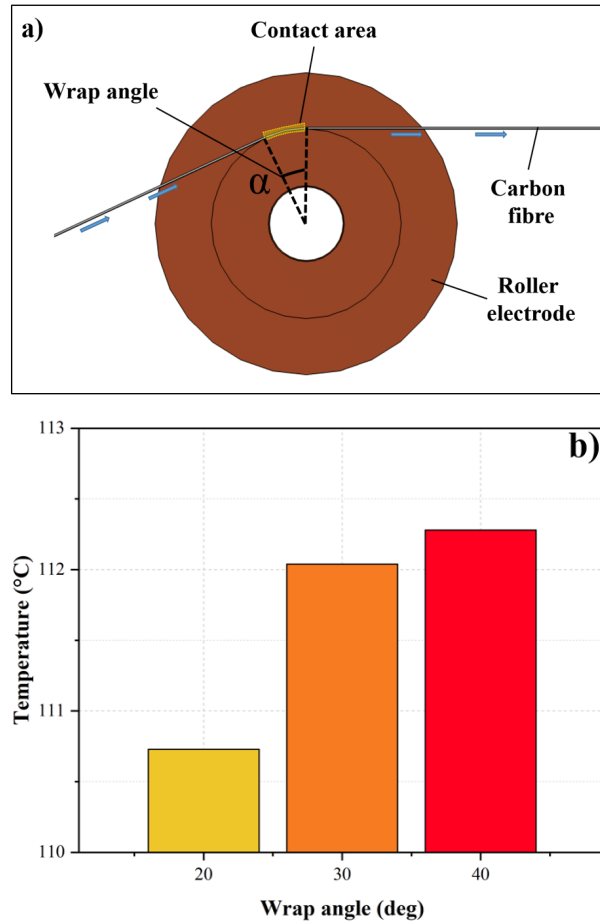
391

392 **Figure 11.** Model predictions of the effect of electrode distance on the maximum temperature at 2 A  
 393 current

394

395 As shown in Figure 12a, the carbon fibre tow contacts the roller electrodes with an angle known as the wrap  
 396 angle. Higher wrap angles increase the contact duration. Assuming the electrical contact resistances linearly  
 397 increase with contact area, the influence of contact resistance heating is expected to be higher at greater wrap  
 398 angles. Moreover, longer contact duration increases the conductive heat transfer between the carbon fibres and  
 399 the roller electrodes. The model was used to evaluate the change in maximum temperature at different wrap  
 400 angles. Figure 12b compares the predicted temperatures for different wrap angles after 60 sec of production,  
 401 where the initial temperature for the rollers and the tow is 20°C. Since electrical contact resistances were not  
 402 experimentally determined for different wrap angles, it was assumed that contact resistance values change  
 403 linearly with the contact area. Kwok and Hahn's [33] measurements from wide and narrow silver paint  
 404 electrodes revealed that electrical contact resistance values varied almost linearly with the contact area of the  
 405 paint. With an increased wrap angle, hence greater contact area, the temperature at the entry region could be  
 406 slightly increased even in a shorter production period than 60 sec. As the roller temperature gradually increases  
 407 due to the contact resistance heating in longer production runs, tow temperature can also further increase due  
 408 to the increased conductive heat transfer from the rollers.

409



410

411

412

413

**Figure 12. a)** Wrap angle representation of the roller electrode **b)** model predictions of the maximum temperature reached after 60 s with respect to different wrap angles

414

#### 4.3. Melting behaviour of powder epoxy

415

416

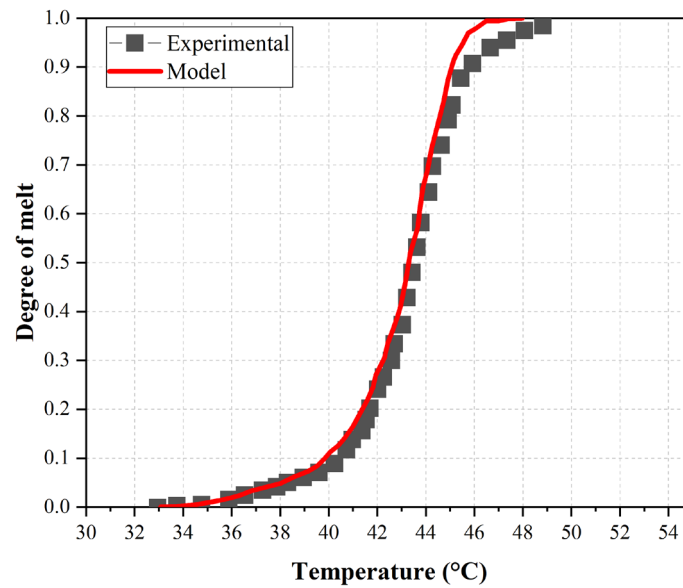
417

418

419

420

It was demonstrated that the melting behaviour of polymer powders can be successfully characterised by using DSC data [43]. The melting of the powder epoxy in the tapeline was modelled by the semi-empirical melting equation Eq. 4 in COMSOL Multiphysics 5.6, where the coefficient and parameters of the equation were obtained by fitting the DSC data by Maguire [56]. The model results showed a good performance in describing the phase change of the powder epoxy as shown in Figure 13, which compares the model predictions to the degree of melt captured by DSC scans by Maguire [56].

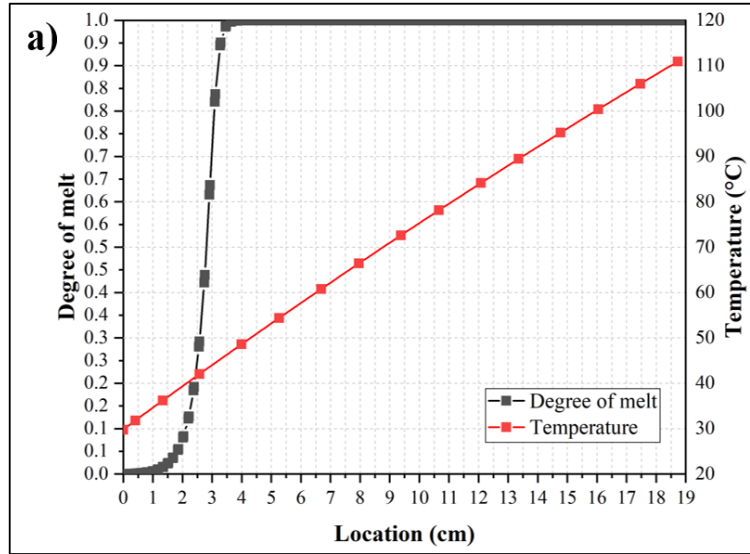


421

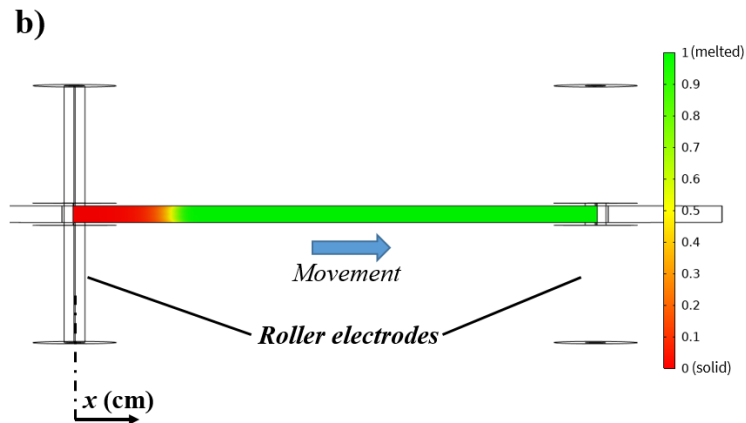
422 **Figure 13.** COMSOL melting model predictions compared with experimental results converted from DSC  
 423 data

424

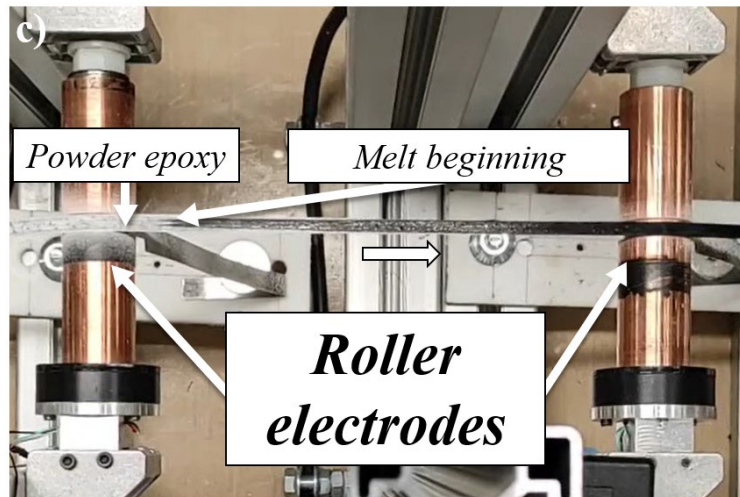
425 The melting model was coupled to the heat transfer model in order to predict when the melting of the  
 426 powder epoxy occurs. The degree of melt, characterised by Eq. 4, is 0 when the powder epoxy is in solid form,  
 427 and 1.0 when it is fully melted. It is important to melt all the powder epoxy as soon as it enters the heating  
 428 section, in order to achieve low viscosity values in the tapeline. The complete melting of the powder epoxy  
 429 can be compromised, particularly at high production speeds, which would lead to incomplete infiltration of  
 430 resin into the carbon fibre tows. The melting model can be used to predict the location at which the melting is  
 431 achieved, and also the optimal power configuration to provide heating. As shown in Figure 14b, powder epoxy  
 432 is predicted to fully melt in the first 3 cm of the heating section, for the given operation conditions (2 A current,  
 433 20 N tension, and 6.5 m/min speed). Similar to section 4.2., a parametric sweep can be carried out in the model  
 434 in order to determine the maximum production speed that can provide melting in the heated section.



435



436



437

438

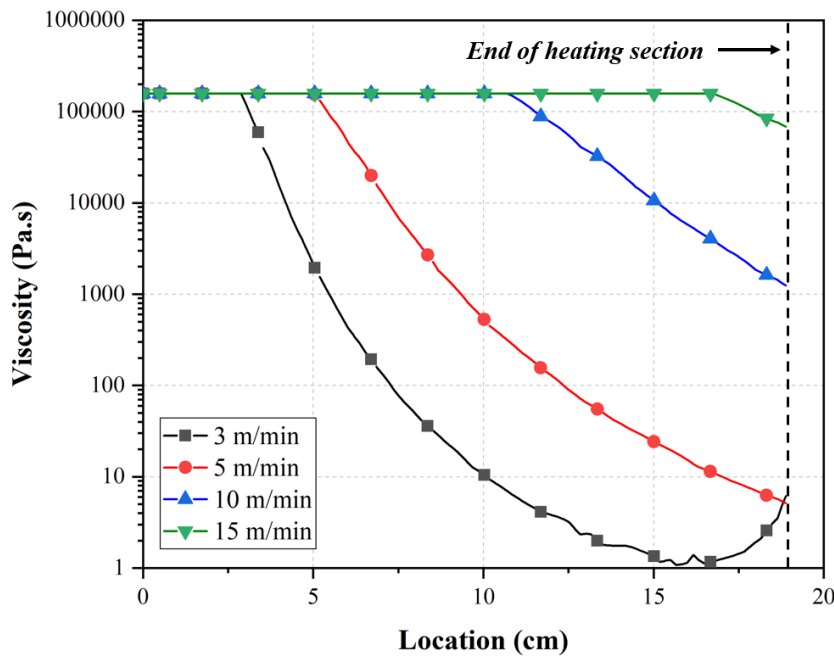
439

440

441

**Figure 14.** a) Model prediction of the degree of melt with respect to temperature for the given production run; b) the degree of melt contours predicted by the model; c) experimental image showing the melting of the powder

442 Increasing the temperature of powder epoxy above the melting point causes the viscosity of the molten  
 443 polymer to decrease. The viscosity of the molten epoxy dictates how the powder particles sinter together and  
 444 also the consolidation behaviour of the towpreg. Lower viscosity values cause molten powder epoxy to flow  
 445 inside the carbon fibre easily, without external pressure. It was demonstrated [57] that the processibility of the  
 446 powder epoxy is ideal at  $\sim 120^{\circ}\text{C}$  when the viscosity is low ( $\sim 1 \text{ Pa}\cdot\text{s}$ ) but the curing rate is slow at this  
 447 temperature. Typically, the operational temperature in the tapeline is kept under  $120^{\circ}\text{C}$  to avoid curing and  
 448 burning additional components (sizing, pigments, fillers etc.) due to momentary surges and overshoots in  
 449 temperature. Viscosity data for the powder epoxy presented in [57] was used in the model to check whether  
 450 the viscosity is predicted to reach ideal conditions in the heating section (Figure 15). The model shows that  
 451 slower production speeds such as 3 m/min (hence, higher temperatures as discussed in Figure 10) will allow  
 452 the resin to reach a minimum viscosity, but the viscosity will begin to increase as the temperature exceeds  
 453  $160^{\circ}\text{C}$  and significant curing will be induced. In contrast, for the given power characteristics, the model shows  
 454 that higher production speeds ( $>10 \text{ m/min}$ ) will not be capable of reducing viscosity to an acceptable value for  
 455 processing in the heating section. To ensure full sintering of the powder epoxy and a good consolidation by  
 456 reaching an ideal viscosity, it is apparent that operating parameters should be adjusted as discussed in section  
 457 4.2.

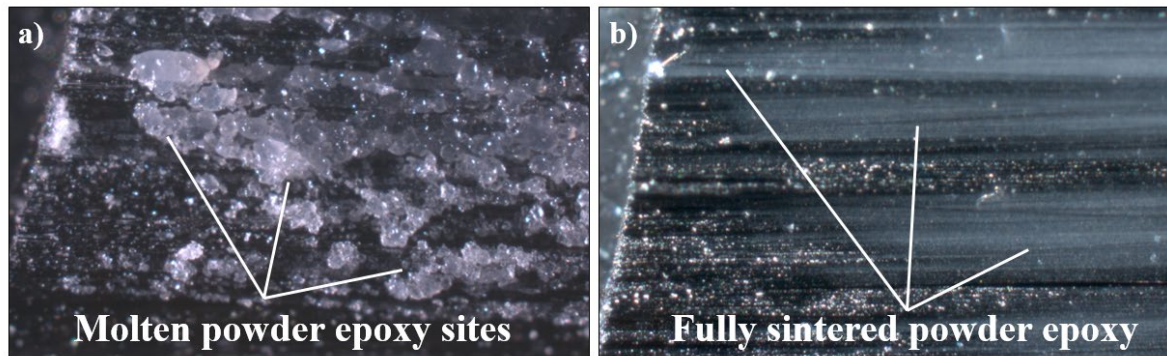


458  
 459 **Figure 15.** Predicted viscosity values along the heating section at different production speeds

460  
 461 *4.4. Sintering of the powder epoxy*

462 The sintering process in the tapeline is a complex phenomenon, which includes inherently  
 463 stochastic parameters such as powder distribution or instantaneous fibre packing of the carbon fibre tows.

464 Sintering results in a more homogenous impregnation, even without an external consolidation pressure. Visual  
465 evidence of the sintering process is presented in Figure 16. The melted and re-solidified (and partially sintered)  
466 powder epoxy on the tow is composed of randomly distributed particles, with different sizes and morphology  
467 (Figure 16a). Further temperature increases beyond the point of sintering will result in viscosity reduction,  
468 followed by coalescence of individual melted powder epoxy sites, creating a uniform and homogenous, void-  
469 free layer (Figure 16b).



470

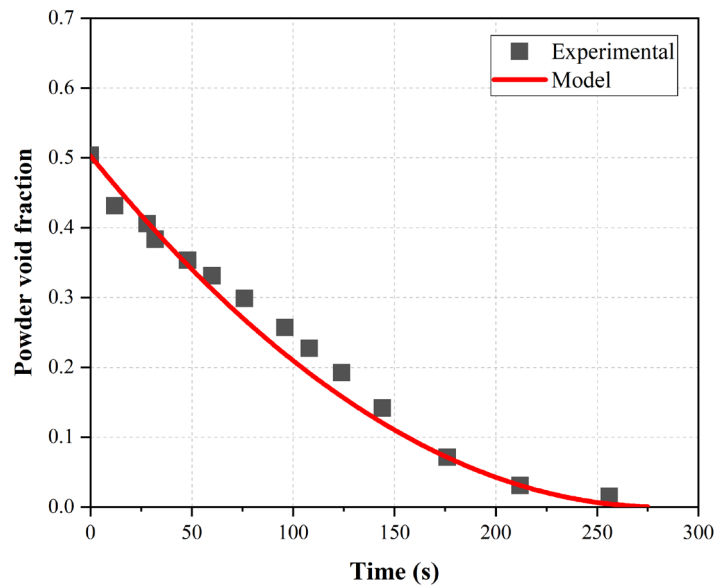
471

**Figure 16.** Sintering process on the towpreg with time and temperature increase

472

473 For the sintering model characterised by Eq. 5, it was assumed that powder epoxy particles do not  
474 flow into the carbon fibre tow while sintering is taking place. Likely, sintering and the beginning of the resin  
475 flow happen concurrently, therefore a consolidation model that can describe the resin flow within the tow is  
476 required to fully understand the relationship between the sintering and the resin flow. This is out of the scope  
477 of this study, however, and Eq. 5 was only used as a simple check to determine if the temperatures reached in  
478 the tapeline are enough to sinter the powder epoxy. In situ experimental determination of the degree of sintering  
479 in the tapeline is difficult, because of this reason, experimental PPR data presented by Maguire et al. [23] was  
480 used to validate the sintering model. The model results showed a good performance in describing the sintering  
481 behaviour of the powder epoxy (Figure 17), and it was coupled to the heat transfer model to analyse sintering  
482 during the production in the tapeline.





483

484

**Figure 17.** Comparison of sintering model predictions with PPR test data given in [23]

485

486

487

488

489

490

491

492

493

494

495

496

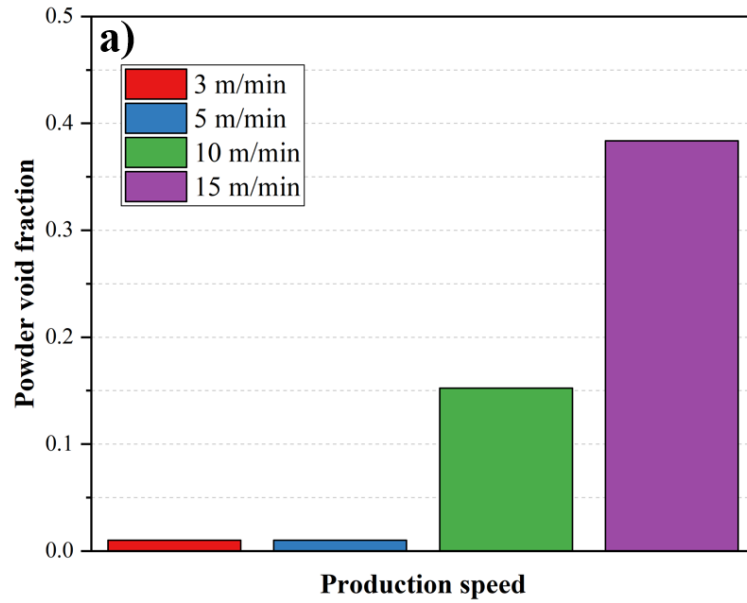
497

498

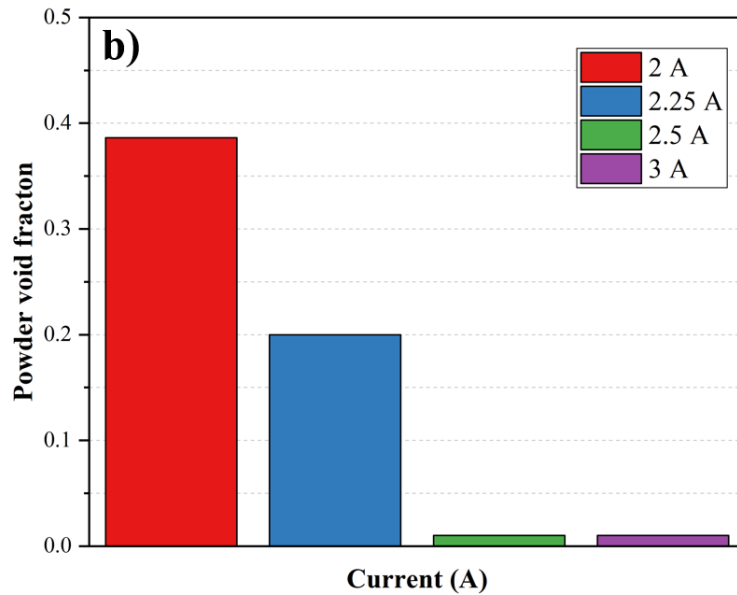
499

500

Sintering is characterised by the thickness change of the polymer bed, which is caused by powder compaction and bubble removal from the interfaces. Eq. 5 predicts the sintering ratio by providing the degree powder void fraction, at a given temperature and time interval. Opposite to the degree of melting parameter, fully sintered powder has a degree of sintering value of  $\chi = 0$ . For the initial sintering state of the powder epoxy, a powder void fraction value of 0.5 was assumed [23]. As a time and temperature-dependent process, sintering in the tapeline also exhibits a similar trend to temperature and melting behaviour. Model predictions reveal that at lower production speeds, 3 and 5 m/min, the powder epoxy on the carbon fibre completely sinters before leaving the heating section (Figure 18a). This result is in line with the viscosity predictions, low viscosities achieved at low production speeds escalate the mobility of molten resin, and powder is completely sintered even in the short time (<10 s) it spends in the heating section. For the higher production speeds, although the powder is completely melted, the powder void fraction at the end of the heating section is 0.15 and 0.38 for 10 and 15 m/min, respectively. These results emphasise the requirement for higher input power at high production speeds. Figure 18b illustrates the model predictions for higher currents at 15 m/min production speed. These results show that it is possible to sinter the powder completely at high production speeds by increasing the supplied power slightly.



501



502

**Figure 18.** Model predictions for minimum degree of powder void fraction reached at **a)** different production speeds and **b)** different currents at 15 m/min production speed

503

504

505

506

## 5. Conclusions

507

508

509

510

511

512

This study demonstrates the analysis capabilities of modelling tools for a powder-epoxy based tapeline. The tapeline aims to produce high-quality, low cost towpregs for AFP applications. The Joule heating system in the line provides an efficient heating system with very low power consumption. An FEA model of the Joule heating system was developed to analyse heating characteristics in detail. The model predictions matched well with the thermal camera captures of the heating process, although small discrepancies were observed due to

513 the temperature variations across the width of the carbon fibre tow, which were caused by tension  
514 inhomogeneity. It was shown that contact resistance heating (CRH) has a significant effect on the tow  
515 temperature at the beginning of the heating zone (entry region). Process parameters, such as power input,  
516 production speed, heating section dimensions and electrode geometry, were analysed in detail using the model  
517 to determine their effects on the heating system. The heat transfer model was coupled to semi-empirical melting  
518 and sintering models to determine optimum conditions for the towpreg production. Results suggest that by  
519 carefully adjusting input power and heating section geometry, desired temperatures can be reached in the  
520 system. Lower production speeds were found to be ideal for more controlled, consistent production runs. As  
521 higher production speeds are targeted in the tapeline (in order to increase production rate and thereby reduce  
522 cost), it was demonstrated that a more powerful power source would be needed. Melting and sintering models  
523 revealed that complete sintering might not be achieved at higher line speeds with the current setup, despite the  
524 powder epoxy being fully melted.

525 Due to the complex nature of the sintering process and its relationship with the consolidation flow, further  
526 resin flow models are required. A consolidation model that is coupled to the presented heat transfer model  
527 would allow analysing the possible concurrent sintering and resin flow into the carbon fibre tow. Investigating  
528 the resin distribution within the carbon fibre tow is crucial to improve the system design for improving the  
529 towpreg quality, which is recommended for future work.

## 530 **6. Acknowledgements**

531

532 This study was part-funded by the UK EPSRC CIMCOMP Future Composites Manufacturing Research  
533 Hub (EP/P006701/1). The first author wishes to express his thanks for the financial support of the Republic of  
534 Turkey Ministry of National Education Scholarship Program.

535

## 536 **7. References**

537 [1] M. N. Grimshaw, C. G. Grant, and J. M. L. Diaz, "Advanced technology tape laying for affordable  
538 manufacturing of large composite structures," *Int. SAMPE Symp. Exhib.*, vol. 46 II, no. 4, pp. 2484–2494,  
539 2001.

540 [2] E. Oromiehie, B. G. Prusty, P. Compston, and G. Rajan, "Automated fibre placement based composite  
541 structures: Review on the defects, impacts and inspections techniques," *Compos. Struct.*, vol. 224, p.  
542 110987, Sep. 2019.

543 [3] A. Brasington, C. Sacco, J. Halbritter, R. Wehbe, and R. Harik, "Automated fiber placement: A  
544 review of history, current technologies, and future paths forward," *Compos. Part C Open Access*, vol. 6,  
545 p. 100182, Oct. 2021.

546 [4] MarketsandMarkets, "Global Prepreg Market by Type of Reinforcement (Carbon Fiber Prepreg,  
547 Glass Fiber Prepreg), Resin Type (Thermoset Prepreg, Thermoplastic Prepreg), Form, Manufacturing  
548 Process (Hot-melt, Solvent Dip), Application, and Region - Forecast to 2025." *Marketresearch.com*, USA,  
549 2021. Accessed: Oct., 24, 2022. [Online]. Available:  
550 [https://www.marketresearch.com/MarketsandMarkets-v3719/Prepreg-Type-Reinforcement-Carbon-](https://www.marketresearch.com/MarketsandMarkets-v3719/Prepreg-Type-Reinforcement-Carbon-Fiber-14311752/)  
551 [Fiber-14311752/](https://www.marketresearch.com/MarketsandMarkets-v3719/Prepreg-Type-Reinforcement-Carbon-Fiber-14311752/)

- 552 [5] H. Diao, P. Robinson, M. R. Wisnom, and A. Bismarck, "Unidirectional carbon fibre reinforced  
553 polyamide-12 composites with enhanced strain to tensile failure by introducing fibre waviness," *Compos.*  
554 *Part A Appl. Sci. Manuf.*, vol. 87, pp. 186–193, Aug. 2016.
- 555 [6] P. Esfandiari, J. F. Silva, P. J. Novo, J. P. Nunes, and A. T. Marques, "Production and processing of  
556 pre-impregnated thermoplastic tapes by pultrusion and compression moulding," *J. Compos. Mater.*, vol.  
557 56, no. 11, pp. 1667–1676, Jun. 2022.
- 558 [7] A. Forcellese, T. Mancina, A. C. Russo, M. Simoncini, and A. Vita, "Robotic automated fiber  
559 placement of carbon fiber towpregs," *Mater. Manuf. Process.*, vol. 37, no. 5, pp. 539–547, 2022.
- 560 [8] R. Arquier, I. Iliopoulos, G. Régnier, and G. Miquelard-Garnier, "Consolidation of continuous-  
561 carbon-fiber-reinforced PAEK composites: a review," *Mater. Today Commun.*, vol. 32, p. 104036, Aug.  
562 2022.
- 563 [9] W. Van De Steene, J. Verstockt, J. Degrieck, K. Ragaert, and L. Cardon, "An evaluation of three  
564 different techniques for melt impregnation of glass fiber bundles with polyamide 12," *Polym. Eng. Sci.*,  
565 vol. 58, no. 4, pp. 601–608, Apr. 2018.
- 566 [10] O. P. L. McGregor, M. Duhovic, A. A. Somashekar, and D. Bhattacharyya, "Pre-impregnated natural  
567 fibre-thermoplastic composite tape manufacture using a novel process," *Compos. Part A Appl. Sci.*  
568 *Manuf.*, vol. 101, pp. 59–71, Oct. 2017.
- 569 [11] S. Wang, Y. Liu, K. Chen, P. Xue, X. Lin, and M. Jia, "Thermal and mechanical properties of the  
570 continuous glass fibers reinforced PVC composites prepared by the wet powder impregnation  
571 technology," *J. Polym. Res.*, vol. 27, no. 4, pp. 1–12, Apr. 2020.
- 572 [12] K. K. C. Ho et al., "Wet impregnation as route to unidirectional carbon fibre reinforced thermoplastic  
573 composites manufacturing," *Plast. Rubber Compos.*, vol. 40, no. 2, pp. 100–107, Mar. 2013.
- 574 [13] M. Asensio et al., "Processing of pre-impregnated thermoplastic towpreg reinforced by continuous  
575 glass fibre and recycled PET by pultrusion," *Compos. Part B Eng.*, vol. 200, p. 108365, Nov. 2020.
- 576 [14] V. Goud, R. Alagirusamy, A. Das, and D. Kalyanasundaram, "Influence of various forms of  
577 polypropylene matrix (fiber, powder and film states) on the flexural strength of carbon-polypropylene  
578 composites," *Compos. Part B Eng.*, vol. 166, pp. 56–64, Jun. 2019.
- 579 [15] V. Goud, R. Alagirusamy, A. Das, and D. Kalyanasundaram, "Dry Electrostatic Spray Coated  
580 Towpregs for Thermoplastic Composites," *Fibers Polym.*, vol. 19, no. 2, pp. 364–374, Feb. 2018.
- 581 [16] V. Goud, A. Ramasamy, A. Das, and D. Kalyanasundaram, "Box-Behnken technique based multi-  
582 parametric optimization of electrostatic spray coating in the manufacturing of thermoplastic composites,"  
583 *Mater. Manuf. Process.*, vol. 34, no. 14, pp. 1638–1645, Oct. 2019.
- 584 [17] A. N. Khan, R. Alagirusamy, P. Mahajan, and A. Das, "Multi-parametric investigation on the  
585 properties of powder-coated UHMWPE /LDPE towpreg manufactured through wet-electrostatic  
586 technique," *Powder Technol.*, vol. 401, Mar. 2022.
- 587 [18] A. N. Khan, V. Goud, R. Alagirusamy, P. Mahajan, and A. Das, "Optimization study on wet  
588 electrostatic powder coating process to manufacture UHMWPE/LDPE towpregs," *J. Ind. Text.*, vol. 51,  
589 pp. 6686S-6704S, Jun. 2022.
- 590 [19] S. Bowman, Q. Jiang, H. Memon, Y. Qiu, W. Liu, and Y. Wei, "Effects of styrene-acrylic sizing on  
591 the mechanical properties of carbon fiber thermoplastic towpregs and their composites," *Molecules*, vol.  
592 23, no. 3, 2018.

- 593 [20] J. P. Nunes and J. F. Siva, "Production of thermoplastic matrix towpregs for highly demanding and  
594 cost-effective commercial applications," *Mater. Sci. Forum*, vol. 730–732, pp. 1030–1035, 2013.
- 595 [21] C. Robert, T. Pecur, J. M. Maguire, A. D. Lafferty, E. D. McCarthy, and C. M. Ó Brádaigh, "A novel  
596 powder-epoxy towpregging line for wind and tidal turbine blades," *Compos. Part B Eng.*, vol. 203, p.  
597 108443, Dec. 2020.
- 598 [22] M. Çelik, T. Noble, F. Jorge, R. Jian, C. M. Ó Brádaigh, and C. Robert, "Influence of Line Processing  
599 Parameters on Properties of Carbon Fibre Epoxy Towpreg," *J. Compos. Sci.* 2022, Vol. 6, Page 75, vol.  
600 6, no. 3, p. 75, Mar. 2022.
- 601 [23] J. M. Maguire, P. Simacek, S. G. Advani, and C. M. Ó Brádaigh, "Novel epoxy powder for  
602 manufacturing thick-section composite parts under vacuum-bag-only conditions. Part I: Through-  
603 thickness process modelling," *Compos. Part A Appl. Sci. Manuf.*, vol. 136, p. 105969, Sep. 2020.
- 604 [24] C. Joseph and C. Viney, "Electrical resistance curing of carbon-fibre/epoxy composites," *Compos.*  
605 *Sci. Technol.*, vol. 60, no. 2, pp. 315–319, Feb. 2000.
- 606 [25] R. L. Sierakowski, I. Y. Telitchev, and O. I. Zhupanska, "On the impact response of electrified carbon  
607 fiber polymer matrix composites: Effects of electric current intensity and duration," *Compos. Sci.*  
608 *Technol.*, vol. 68, no. 3–4, pp. 639–649, Mar. 2008.
- 609 [26] A. E. Zantout and O. I. Zhupanska, "On the electrical resistance of carbon fiber polymer matrix  
610 composites," *Compos. Part A Appl. Sci. Manuf.*, vol. 41, no. 11, pp. 1719–1727, Nov. 2010.
- 611 [27] N. Athanasopoulos, G. Koutsoukis, D. Vlachos, and V. Kostopoulos, "Temperature uniformity  
612 analysis and development of open lightweight composite molds using carbon fibers as heating elements,"  
613 *Compos. Part B Eng.*, vol. 50, pp. 279–289, Jul. 2013.
- 614 [28] X. Xu et al., "In-situ curing of glass fiber reinforced polymer composites via resistive heating of  
615 carbon nanotube films," *Compos. Sci. Technol.*, vol. 149, pp. 20–27, Sep. 2017.
- 616 [29] S. A. Hayes, A. D. Lafferty, G. Altinkurt, P. R. Wilson, M. Collinson, and P. Duchene, "Direct  
617 electrical cure of carbon fiber composites," *Adv. Manuf. Polym. Compos. Sci.*, vol. 1, no. 2, pp. 112–119,  
618 Apr. 2015.
- 619 [30] S. J. Joo, M. H. Yu, W. S. Kim, and H. S. Kim, "Damage detection and self-healing of carbon fiber  
620 polypropylene (CFPP)/carbon nanotube (CNT) nano-composite via addressable conducting network,"  
621 *Compos. Sci. Technol.*, vol. 167, pp. 62–70, Oct. 2018.
- 622 [31] J. Orellana, I. Moreno-villoslada, R. K. Bose, F. Picchioni, M. E. Flores, and R. Araya-hermosilla,  
623 "Self-healing polymer nanocomposite materials by joule effect," *Polymers*, vol. 13, no. 4, pp. 1–24, 2021.
- 624 [32] B. Mas, J. P. Fernández-Blázquez, J. Duval, H. Bunyan, and J. J. Vilatela, "Thermoset curing through  
625 Joule heating of nanocarbons for composite manufacture, repair and soldering," *Carbon N. Y.*, vol. 63,  
626 pp. 523–529, Nov. 2013.
- 627 [33] N. Kwok and H. T. Hahn, "Resistance Heating for Self-healing Composites," *J. Compos. Mater.*,  
628 vol. 41, no. 13, pp. 1635–1654, Jul. 2007.
- 629 [34] J. Seyyed Monfared Zanjani, B. Saner Okan, P. N. Pappas, C. Galiotis, Y. Z. Menciloglu, and M.  
630 Yildiz, "Tailoring viscoelastic response, self-heating and deicing properties of carbon-fiber reinforced  
631 epoxy composites by graphene modification," *Compos. Part A Appl. Sci. Manuf.*, vol. 106, pp. 1–10, Mar.  
632 2018.

633 [35]N. Athanasopoulos, D. Sikoutris, T. Panidis, and V. Kostopoulos, “Numerical investigation and  
634 experimental verification of the Joule heating effect of polyacrylonitrile-based carbon fiber tows under  
635 high vacuum conditions,” *J. Compos. Mater.*, vol. 46, no. 18, pp. 2153–2165, Aug. 2012.

636 [36]N. Athanasopoulos and V. Kostopoulos, “Resistive heating of multidirectional and unidirectional dry  
637 carbon fibre preforms,” *Compos. Sci. Technol.*, vol. 72, no. 11, pp. 1273–1282, Jun. 2012.

638 [37]A. T. Chien, S. Cho, Y. Joshi, and S. Kumar, “Electrical conductivity and Joule heating of  
639 polyacrylonitrile/carbon nanotube composite fibers,” *Polymer (Guildf.)*, vol. 55, no. 26, pp. 6896–6905,  
640 Dec. 2014.

641 [38]Y. Grohmann, “Continuous Resistance Heating Technology for High-Speed Carbon Fibre Placement  
642 Processes,” in *SAMPE Europe 2020*, 2020, pp. 3–12.

643 [39]M. Lu et al., “Continuous stabilization of polyacrylonitrile (PAN) - carbon nanotube (CNT) fibers by  
644 Joule heating,” *Chem. Eng. Sci.*, vol. 236, p. 116495, Jun. 2021.

645 [40]M. Kontopoulou and J. Vlachopoulos, “Melting and densification of thermoplastic powders,” *Polym.*  
646 *Eng. Sci.*, vol. 41, no. 2 SPEC. ISS, pp. 155–169, Feb. 2001.

647 [41]C. T. Bellehumeur and J. S. Tiang, “Simulation of non-isothermal melt densification of polyethylene  
648 in rotational molding,” *Polym. Eng. Sci.*, vol. 42, no. 1, pp. 215–229, 2002.

649 [42]C. T. Bellehumeur, M. K. Bisaria, and J. Vlachopoulos, “An experimental study and model  
650 assessment of polymer sintering,” *Polym. Eng. Sci.*, vol. 36, no. 17, pp. 2198–2207, 1996.

651 [43]A. Greco and A. Maffezzoli, “Polymer melting and polymer powder sintering by thermal analysis,”  
652 *J. Therm. Anal. Calorim.*, vol. 72, no. 3, pp. 1167–1174, 2003.

653 [44]M. Kandis and T. L. Bergman, “Observation, Prediction, and Correlation of Geometric Shape  
654 Evolution Induced by Non-Isothermal Sintering of Polymer Powder,” *J. Heat Transfer*, vol. 119, no. 4,  
655 pp. 824–831, Nov. 1997.

656 [45]M. Çelik et al., “Contact resistance heating of unidirectional carbon fibre tows in a powder-epoxy  
657 towpregging line,” *Plast. Rubber Compos.*, pp. 1–10, 2022.

658 [46]M. Sandberg, O. Yuksel, I. Baran, J. Spangenberg, and J. H. Hattel, “Steady-state modelling and  
659 analysis of process-induced stress and deformation in thermoset pultrusion processes,” *Compos. Part B*  
660 *Eng.*, vol. 216, p. 108812, Jul. 2021.

661 [47]M. Volk, J. Wong, S. Arreguin, and P. Ermanni, “Pultrusion of large thermoplastic composite profiles  
662 up to Ø 40 mm from glass-fibre/PET commingled yarns,” *Compos. Part B Eng.*, vol. 227, Dec. 2021.

663 [48]K. Minchenkov et al., “Effects of the quality of pre-consolidated materials on the mechanical  
664 properties and morphology of thermoplastic pultruded flat laminates,” *Compos. Commun.*, vol. 35, Nov.  
665 2022.

666 [49]A. Trende, B. T. Åström, A. Wöginger, C. Mayer, and M. Neitzel, “Modelling of heat transfer in  
667 thermoplastic composites manufacturing: double-belt press lamination,” *Compos. Part A Appl. Sci.*  
668 *Manuf.*, vol. 30, no. 8, pp. 935–943, 1999.

669 [50]K. Deng, C. Zhang, X. Dong, and K. K. Fu, “Rapid and energy-efficient manufacturing of thermoset  
670 prepreg via localized in-plane thermal assist (LITA) technique,” *Compos. Part A Appl. Sci. Manuf.*, vol.  
671 161, p. 107121, Oct. 2022.

672 [51]B. Shi et al., “Dynamic Capillary-Driven Additive Manufacturing of Continuous Carbon Fiber  
673 Composite,” *Matter*, vol. 2, no. 6, pp. 1594–1604, Jun. 2020.

- 674 [52] A. Vashisth, R. E. Healey, M. J. Pospisil, J. H. Oh, and M. J. Green, "Continuous processing of pre-  
675 preregs using radio frequency heating," *Compos. Sci. Technol.*, vol. 195, p. 108211, Jul. 2020.
- 676 [53] Toray, "Toray T700S Standard Modulus Carbon Fiber." p. 2, 2018.
- 677 [54] COMSOL AB, "COMSOL Multiphysics® v. 5.6." Stockholm, Sweden.
- 678 [55] E. B. Jeon, T. Fujimura, K. Takahashi, and H. S. Kim, "An investigation of contact resistance between  
679 carbon fiber/epoxy composite laminate and printed silver electrode for damage monitoring," *Compos. Part  
680 A Appl. Sci. Manuf.*, vol. 66, pp. 193–200, Nov. 2014.
- 681 [56] J. M. Maguire, "Processing of Thick Section Epoxy Powder Composite Structures," PhD dissertation,  
682 The University of Edinburgh, 2019.
- 683 [57] J. M. Maguire, K. Nayak, and C. M. Ó Brádaigh, "Characterisation of epoxy powders for processing  
684 thick-section composite structures," *Mater. Des.*, vol. 139, pp. 112–121, Feb. 2018.